Research Article

Bo Hou, Aiqin Wang*, Pei Liu*, and Jingpei Xie

Investigation of the nucleation and growth behavior of Ti₂AlC and Ti₃AlC nano-precipitates in TiAl alloys

https://doi.org/10.1515/ntrev-2022-0510 received July 11, 2022; accepted January 3, 2023

Abstract: In this work, the nucleation and growth behavior of Ti₂AlC and Ti₃AlC nano-precipitates in Ti-44Al-1.2C alloys were systematically studied by observing their distribution, morphology, and interface atomic structure. The experiment results show that the needle-like C atom segregation zones in TiAl alloys are the nucleation site of Ti₂AlC, and the long axis direction of segregation zones is parallel to the TiAl(111) plane. The rod-like Ti₂AlC nano-precipitates mainly distribute at the TiAl/Ti₃Al interface, and the orientation relationship between them is $[\overline{1}01]$ TiAl/ $[11\overline{2}0]$ $Ti_2AlC//[11\overline{2}0]Ti_3Al$, $(111)TiAl//(0001)Ti_2AlC//(0001)Ti_3Al$. The needle-like Ti₃AlC nano-precipitates distribute in TiAl with the orientation relationship of [001]Ti₃AlC// [001]TiAl, (100)Ti₃AlC//(100)TiAl, (020)Ti₃AlC//(020)TiAl, and (110)Ti₃AlC//(110)TiAl during the nucleation stage. After growing into the rod-like, the orientation relationship between Ti₃AlC precipitates and TiAl is [1\overline{11}0]Ti₃AlC//[1\overline{10}0] TiAl, (001)Ti₃AlC//(001)TiAl, (220)Ti₃AlC//(220)TiAl, and (111)Ti₃AlC//(111)TiAl. Both the needle- and rod-like Ti₃AlC

precipitates preferentially grow along the [001]TiAl direction. The crystal structure and lattice mismatch between Ti_2AlC and Ti_3AlC nano-precipitates and the TiAl matrix determine their distribution, morphology, and interface atomic structure.

Keywords: TiAl alloys, Ti₂AlC and Ti₃AlC nano-precipitates, nucleation and growth, interface atomic structure

1 Introduction

The requirements for engine performance have become increasingly stringent due to the rapid development of the aerospace and automotive fields in recent years, i.e., lighter, stronger, and higher. The development of new lightweight, high-temperature structural materials has become the key to improving engine performance and reducing energy consumption. TiAl alloys are expected to become the competitive high-temperature structural materials to replace nickel-based superalloys at the service temperature of 650-850°C due to their high melting point, low density, high specific strength, and specific modulus [1–7]. Nevertheless, the practical application of TiAl alloys at room temperature (<2%) was limited due to their poor ductility. To overcome the aforementioned shortcomings, researchers discovered that alloying technology is a reliable method to enhance the mechanical properties of TiAl alloys. In addition to the commonly used metallic elements (Nb, Cr, and B), the infinitesimal non-metallic elements (C, N, and O) can also have an effect on the microstructure and mechanical properties of TiAl alloys [8-12].

Domestic and foreign studies have shown that the C atom could refine the microstructure by changing the solidification path of TiAl alloys and could also improve their strength and creep resistance through solid solution strengthening and precipitation strengthening [13,14]. Noteworthy is the fact that the effect of precipitation strengthening is related to the C content. Wang *et al.* [15] found that the room temperature tensile properties

Bo Hou: College of Materials Science and Engineering, Henan University of Science and Technology, Luoyang 471023, China Jingpei Xie: College of Materials Science and Engineering, Henan University of Science and Technology, Luoyang 471023, China; Provincial and Ministerial Co-construction of Collaborative Innovation Center for Non-ferrous Metal New Materials and Advanced Processing Technology, Luoyang 471023, China

^{*} Corresponding author: Aiqin Wang, College of Materials Science and Engineering, Henan University of Science and Technology, Luoyang 471023, China; Provincial and Ministerial Co-construction of Collaborative Innovation Center for Non-ferrous Metal New Materials and Advanced Processing Technology, Luoyang 471023, China, e-mail: aiqin_wang888@163.com

^{*} Corresponding author: Pei Liu, College of Materials Science and Engineering, Henan University of Science and Technology, Luoyang 471023, China; Provincial and Ministerial Co-construction of Collaborative Innovation Center for Non-ferrous Metal New Materials and Advanced Processing Technology, Luoyang 471023, China, e-mail: liupei@haust.edu.cn

of Ti-47Al-2Nb-2Cr could be significantly improved when the C content reaches 0.2 at.%. Li et al. [16] also found that 0.5 at.% C content could simultaneously improve the ultimate tensile strength and elongation of the Ti-43Al-6Nb-1Mo-1Cr alloy. Previous studies have shown that the C atom has a solid solution limit in TiAl alloys, and its solid solubility is greatly affected by factors such as temperature and alloying elements [17,18]. When the C content exceeds the solid solution limit of TiAl alloys, two kinds of carbides will precipitate, i.e., Ti₂AlC and Ti₃AlC. Schwaighofer et al. [19] found that the addition of C could cause the precipitation of the fine Ti₂AlC carbides in TiAl alloys. Wu et al. [20] proved that both the fine Ti₂AlC and Ti₃AlC carbides could precipitate from C-containing TiAl alloys, and the carbide precipitates could also refine the microstructure of the TiAl matrix. Lapin et al. [21] studied the high-temperature deformation behavior of C-containing TiAl alloys and found that the fine Ti₂AlC and Ti₃AlC carbide precipitates could improve the creep resistance of TiAl alloys by hindering the movement of dislocations. Based on the aforementioned analysis, it could be seen that the precipitation of Ti₂AlC and Ti₃AlC carbides significantly improves the microstructure and mechanical properties of TiAl alloys, necessitating further research into their precipitation (nucleation and growth) behavior. However, according to our knowledge, the correlative investigation has not been reported up to date.

In the present work, the distribution, morphology, and interface atomic structure of Ti₂AlC and Ti₃AlC nanoprecipitates in Ti–44Al–1.2C alloys were systematically observed using transmission electron microscopy (TEM), and the nucleation and growth behavior of two carbides in TiAl alloys were concluded. This study has a guiding significance for controlling the morphology and distribution of Ti₂AlC and Ti₃AlC nano-precipitates and contributes to optimizing the mechanical properties of TiAl alloys.

2 Experimental methods

In this study, spherical Ti powder (99.95% purity, ~25 μ m), spherical Al powder (99.95% purity, ~25 μ m), and graphene nanosheets were used as raw materials for the preparation of carbon-containing TiAl alloys. The Ti/Al/C composite powders were obtained by a high-energy ball milling equipment with argon gas protection based on the atomic ratio of Ti-44Al-1.2C. Afterward, the composite powders placed in a graphite mold were compacted through the pneumatic press, and then the carbon-containing TiAl alloy sample was prepared by vacuum hot

pressing sintering at 1,623 K with 40 MPa for 2h. The TiAl alloy sample was cut into a sample of 10 \times 10 \times 10 mm³, and the solution was treated at 1,523 K for 20 h and aged at 1,173 K for 1 h. It is worth emphasizing that in order to prevent the alloy from oxidizing at high temperatures, the heat treatment process is carried out in a quartz tube filled with argon as a protective gas. The microstructure and element distribution were characterized by scanning electron microscopy (SEM, JSM-7800F) coupled with energy dispersive spectroscopy. The cylindrical specimens with the size of $\Phi6 \, \text{mm} \times 9 \, \text{mm}$ were used for the roomtemperature compression tests by an electronic universal material testing machine (ZUAG-I250 KN). The high-temperature compression tests of the TiAl alloys with the same cylindrical size were carried out on the Gleeble-3800 system with a strain rate of 0.001 s⁻¹. The sample for TEM analysis was machined into 0.5 mm from the aged sample using wire-electrode cutting and mechanically ground to about 60 µm, then cut into 3-mm-diameter foils. The Gatan precision ion polishing system (Gatan Model 695) was used for further thinning, and morphology analysis and phase identification were carried out by TEM (JEM-2100) with an accelerating voltage of 300 kV.

3 Results and analysis

3.1 Microstructure and mechanical properties

Figure 1(a)–(c) shows the SEM microstructure and corresponding elemental point analysis of TiAl alloys after heat treatment, respectively, and it could be observed that the TiAl matrix consists of TiAl and Ti₃Al phases in the form of lamellar colonies. Figure 1(d) shows the roomtemperature compressive stress-strain curve of the TiAl alloys, and the results indicated that the compressive strength is about 1,591 MPa and the compressive strain is about 16.7%. As can be seen from the true stress-strain curve in the inset, the true stress increases with an increasing strain rate. The true stress increases sharply with the increase in deformation strain in the initial stage and then increases slowly to the highest point of true stress. In addition, as shown in Figure 1(e), the compressive strength of the TiAl alloys at 800°C is about 639 MPa. The room-temperature and high-temperature compressive performances of this work are at a middle level among the reported TiAl alloys and TiAl-based composites, which may be related to the carbon content, sintering temperature, and time.

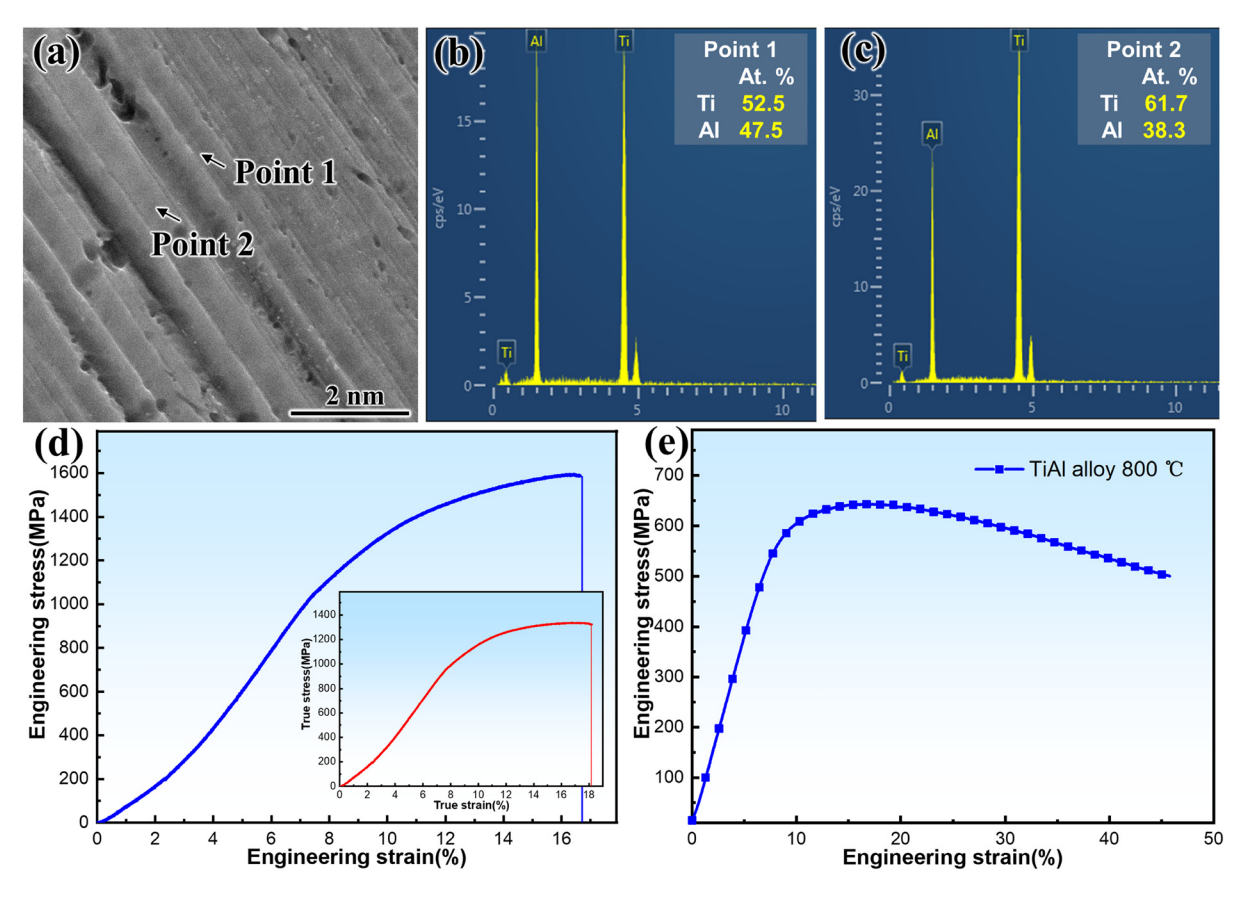


Figure 1: The SEM microstructure and mechanical properties of TiAl alloys: (a) SEM image; (b) element composition of Point 1 in (a); (c) element composition of Point 2 in (a); (d) room-temperature compressive stress-strain curve; and (e) high-temperature compressive stress-strain curve.

3.2 Nucleation and growth behavior of Ti₂AlC nano-precipitates in TiAl alloys

Figure 2(a) shows the high-resolution transmission electron microscopy (HRTEM) morphology of the needle-like

C atom segregation zones in TiAl, and Figure 2(b) is the fast Fourier transform (FFT) pattern of the square area in Figure 2(a). According to the calibration result in Figure 2(b), it could be seen that quite a few segregation zones in Figure 1(a) distribute parallel to each other along the TiAl

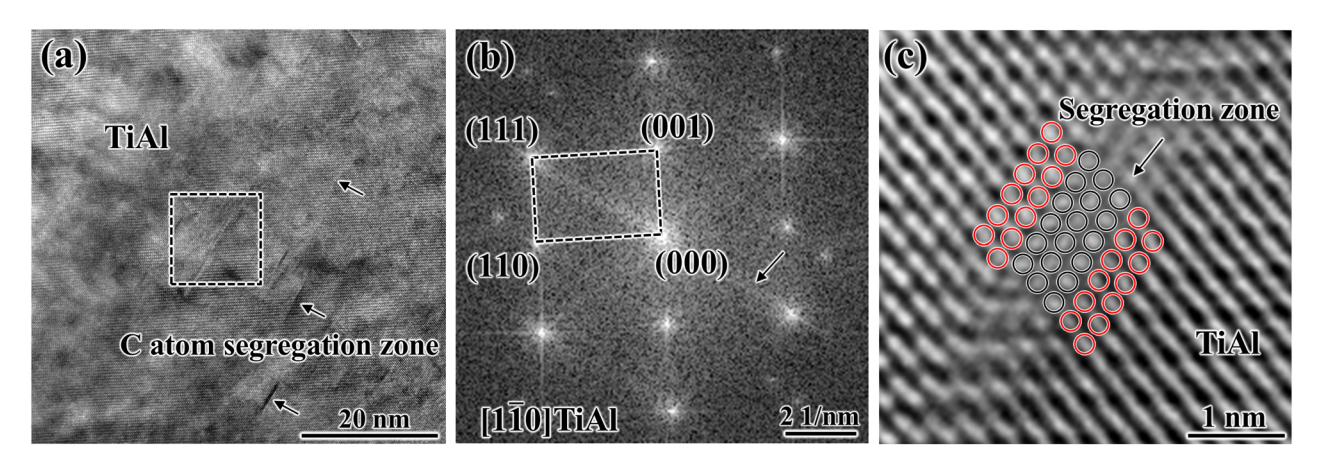


Figure 2: The TEM analysis of C atom segregation in TiAl alloys. (a) HRTEM image of segregation zone; (b) FFT pattern; and (c) IFFT image of segregation zone.

(111). It could be observed from the inverse FFT (IFFT) image in Figure 2(c) that the segregation zone is only a few unit cells wide and its lattice arrangement is distorted to a certain extent compared with the surrounding TiAl matrix. Based on the morphology and crystallographic knowledge, we consider that the C atom segregation zone nucleates on TiAl(111) and then grows along TiAl (111) to be needle-like. In addition, we also think that as C atoms continue to segregate, this region will transform into Ti₂AlC nano-precipitates, which will be discussed in detail in Section 4.

Figure 3 shows the nucleation and growth behavior of rod-like Ti_2AlC nano-precipitates precipitated from the $TiAl/Ti_3Al$ interface. As seen in Figure 3(a), the $TiAl/Ti_3Al$ matrix consists of lamellae γ -TiAl and lamellae α_2 - Ti_3Al , and also found that a small number of rod-like Ti_2AlC nano-precipitates distribute at the $TiAl/Ti_3Al$ interface. Figure 3(b) shows the HRTEM image of the square area in Figure 3(a), and it could be observed that the width of the Ti_2AlC nano-precipitate is about 10 nm. Insets (b-1), (b-2), and (b-3) in Figure 3(b) are the FFT patterns corresponding to

 Ti_3Al , Ti_2AlC , and TiAl, respectively. According to the calibration results, it could be determined that inset (b-1) is the TiAl along the $[\bar{1}01]$ zone axis, inset (b-2) is the Ti_2AlC along the $[11\bar{2}0]$ zone axis, and inset (b-3) is the Ti_3Al along the $[11\bar{2}0]$ zone axis. The FFT pattern of the $TiAl/Ti_2AlC/Ti_3Al$ interface is shown in Figure 3(c), and the corresponding indexed pattern of Figure 3(c) is shown in Figure 3(d). According to the calibration result in Figure 3(d), their orientation relationship is as follows:

 $\begin{array}{lll} [\overline{1}01]TiAl//[11\overline{2}0]Ti_{2}AlC//[11\overline{2}0]Ti_{3}Al, \ (111)TiAl//(0001) \\ Ti_{2}AlC//(0001)Ti_{3}Al. \end{array}$

Figure 3(e) and (f) shows the IFFT images of the square area 1 and 2 in Figure 3(b), respectively. The IFFT images were marked to see the atomic arrangement of the interface more clearly, as shown in Figure 3(e)–(f), where the following red, purple, and blue circles represent the TiAl atoms, Ti_2AlC atoms, and Ti_3Al atoms, respectively. Figure 3(f) exhibits that the atomic stacking sequence of Ti_2AlC can be regarded as the sequence of BABABAB along the [0001] direction, where the underlined letters correspond to Al layers and the non-

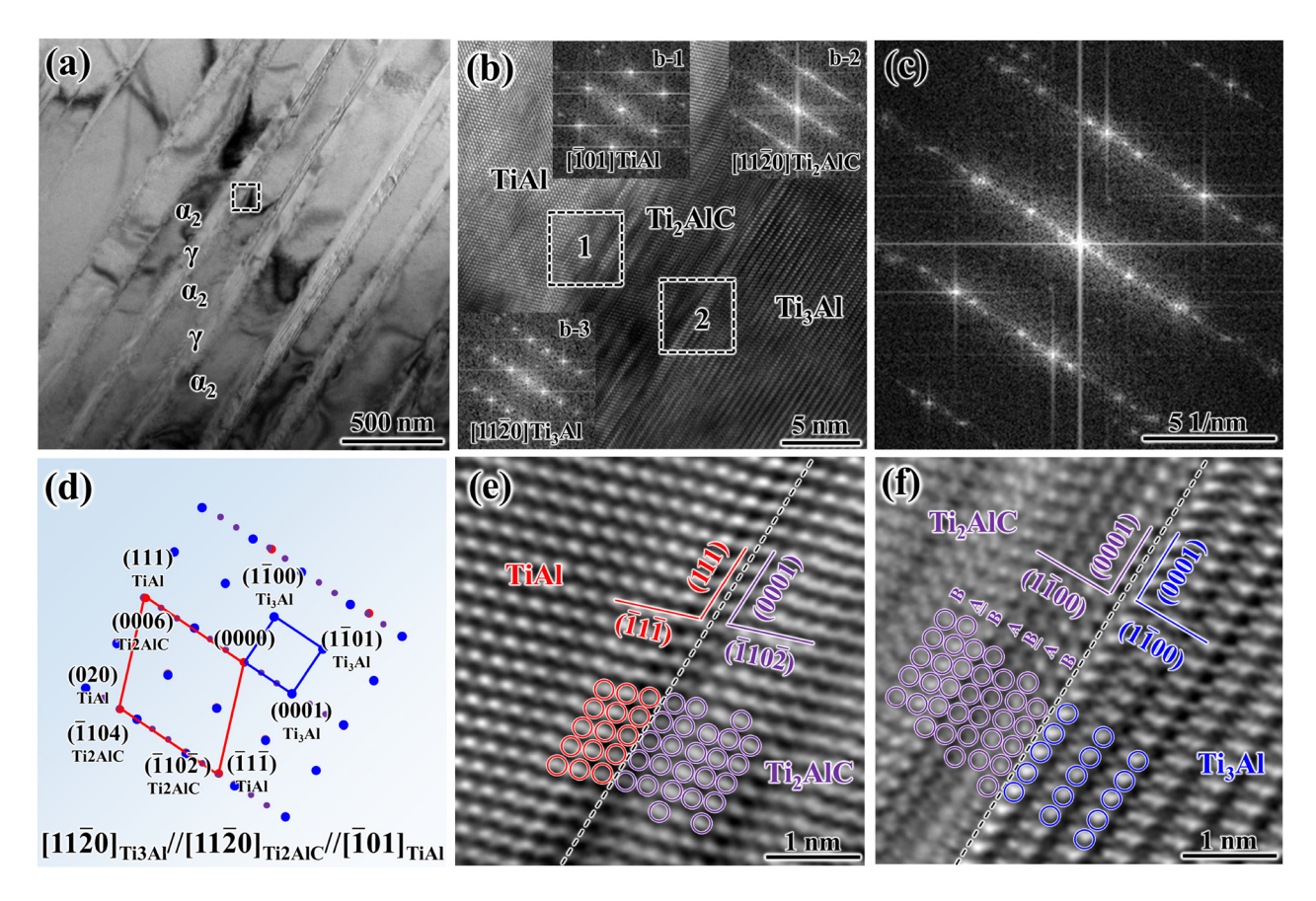


Figure 3: The TEM analysis of rod-like Ti₂AlC nano-precipitates at the TiAl/Ti₃Al interface: (a) TEM image of TiAl/Ti₃Al and rod-like Ti₂AlC; (b) HRTEM image of the TiAl/Ti₂AlC/Ti₃Al interface; (c) FFT pattern of the TiAl/Ti₂AlC/Ti₃Al interface; (d) indexing of the FFT pattern in (c); (e) IFFT image of the Ti₂AlC/TiAl interface; and (f) IFFT image of the Ti₃Al/Ti₂AlC interface.

underlined letters correspond to Ti layers, and the result is consistent with the previously studied layered crystal structure of Ti₂AlC [22–24]. Furthermore, based on the arrangement of interface atoms, it could be concluded that both the Ti₂AlC/TiAl interface and the Ti₃Al/Ti₂AlC interface show good atomic matching, indicating that these interfaces are coherent.

In addition to the precipitation of rod-like Ti₂AlC at the TiAl/Ti₃Al interface, the rod-like Ti₂AlC nano-precipitate could also be observed in Ti₃Al, as shown in Figure 4(a). Figure 4(b) shows the HRTEM image of the Ti₃Al/ Ti₂AlC interface, and the insets (b-1) and (b-2) are the corresponding FFT patterns of Ti₃Al and Ti₂AlC, respectively. It could be determined from the calibration results that inset (b-1) is the Ti_3Al along the $[11\overline{2}0]$ zone axis and inset (b-2) is the Ti₂AlC along the [1120] zone axis. Figure 4(c) shows the FFT pattern of the Ti₃Al/Ti₂AlC interface, and Figure 4(d) is the corresponding indexed pattern of Figure 4(c). Figure 4(e) and (f) is both IFFT images of the Ti₃Al/Ti₂AlC interface, and atomic arrangement results indicate that the orientation relationship between Ti₃Al and Ti_2AlC is the same as that in Figure 3(e), i.e., [11 $\overline{2}0$] $Ti_3Al//[11\overline{2}0]Ti_2AlC$ and $(0001)Ti_3Al//(0001)Ti_2AlC$.

3.3 Nucleation and growth behavior of Ti₃AlC nano-precipitates in TiAl alloys

Apart from the distribution of Ti_2AlC nano-precipitates in TiAl alloys, we also observed the precipitation of needle-like Ti_3AlC , as shown in Figure 5(a). It could be seen that the high-density needle-like Ti_3AlC nano-precipitates in TiAl alloys are distributed parallel to each other, and there are numerous dislocations around them. Figure 5(b) shows the HRTEM image of needle-like Ti_3AlC nano-precipitates in TiAl, and Figure 5(c) is the FFT pattern of the square area in Figure 5(b). The calibration result shows that the TiAlC corresponds to the ICC zone axis, and it could be determined that the Ti_3AlC nano-precipitates grow needle-like along the TiAl[001] direction according to the morphology in Figure 5(b).

Based on the aforementioned analysis, it could be observed that the needle-like Ti_3AlC nano-precipitates grow along the TiAl[001] direction. Therefore, the needle-like Ti_3AlC nano-precipitates show dot-like cross-sections when imaged along the TiAl[001] direction, and the corresponding TEM images were shown in Figure 6(a) and (b). Figure 6(c) shows the HRTEM image of the needle-like Ti_3AlC

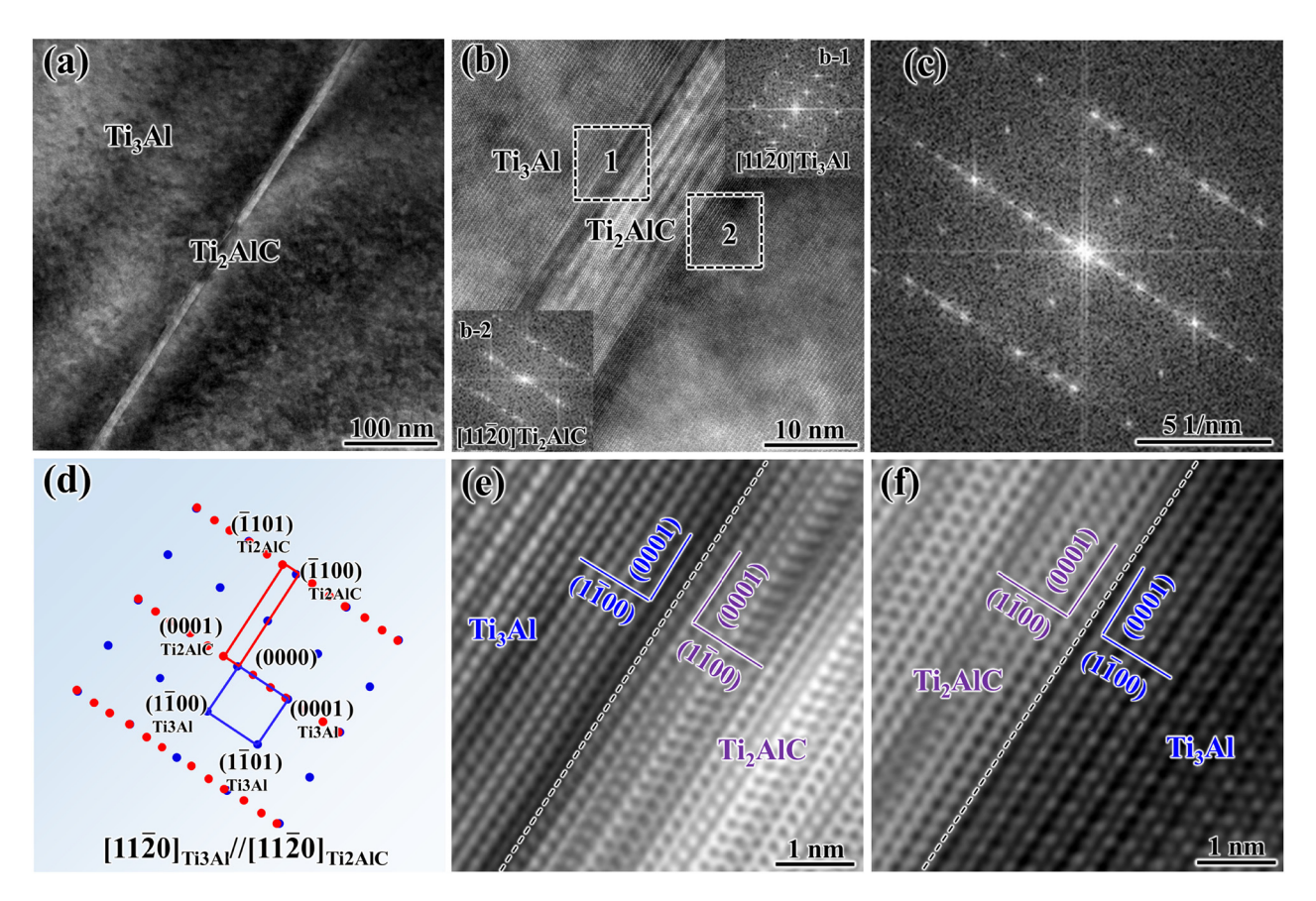


Figure 4: The TEM analysis of rod-like Ti₂AlC nano-precipitate in Ti₃Al: (a) TEM image of Ti₂AlC in Ti₃Al; (b) HRTEM image of the Ti₃Al/Ti₂AlC interface; (c) FFT pattern of the Ti₃Al/Ti₂AlC interface; (d) indexing of the FFT pattern in (c); and (e and f) IFFT images of the Ti₃Al/Ti₂AlC interface.

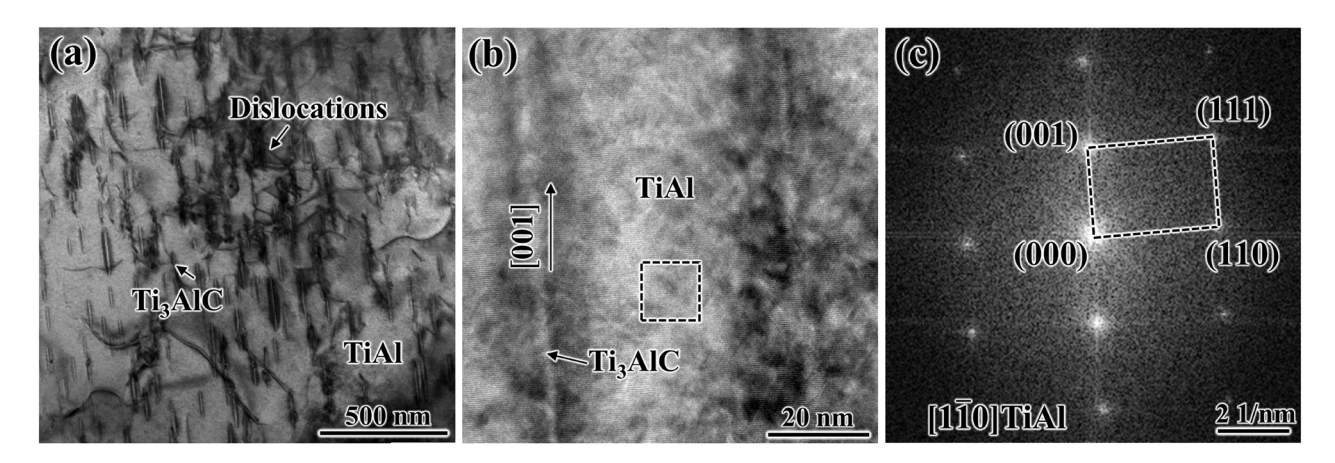


Figure 5: The TEM analysis of needle-like Ti₃AlC nano-precipitates in TiAl alloys: (a) TEM image of needle-like Ti₃AlC in TiAl; (b) HRTEM image of needle-like Ti₃AlC in TiAl; (c) FFT pattern of TiAl.

nano-precipitates, where the TiAl is on the right side of the image. Figure 6(d) is the FFT pattern of the square area in Figure 6(c), and it can be seen that the diffraction spots of Ti₃AlC appear between the diffraction spots of TiAl. The diffraction spots of Ti₃AlC phase exist in the TiAl phase, which is due to the lattice parameters of Ti₃AlC and TiAl

being quite similar, thereby the diffraction spots of Ti_3AlC appear at the superlattice position of TiAl with the face-centered tetragonal structure, which also proves the formation of Ti_3AlC nano-precipitates from TiAl. The corresponding index pattern of Figure 6(d) is shown in Figure 6(e), and the calibration result shows that the Ti_3AlC is along the

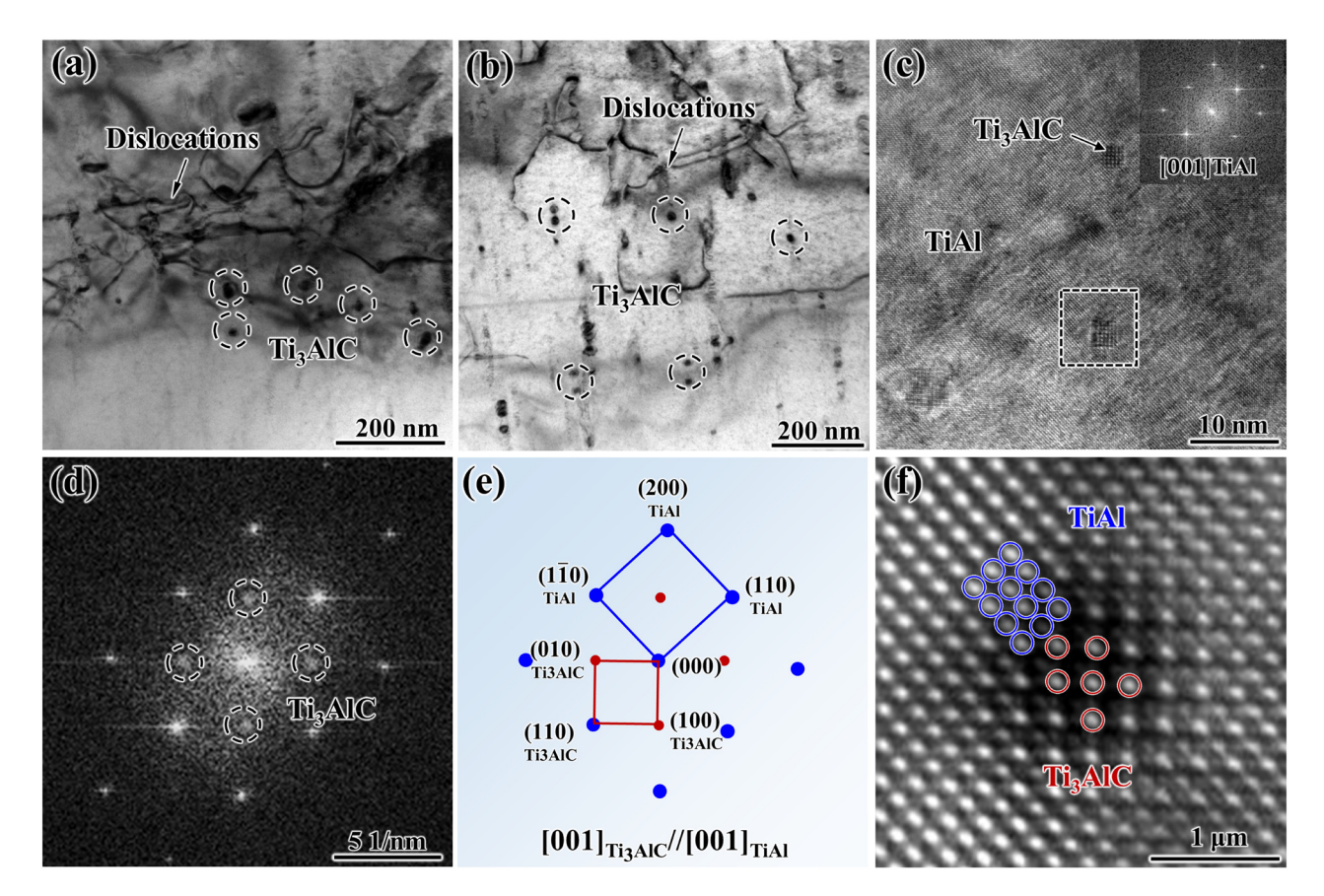


Figure 6: The TEM analysis of needle-like Ti₃AlC nano-precipitates in TiAl alloys: (a and b) TEM images; (c) HRTEM image; (d) FFT pattern of the square area in (c); (e) indexing of the FFT pattern in (d); and (f) IFFT image of the square area in (c).

[001] zone axis, the TiAl is along the [001] zone axis, the $Ti_3AlC(100)$ is parallel to the TiAl(100), the $Ti_3AlC(020)$ is parallel to the TiAl(020), and the $Ti_3AlC(110)$ is parallel to the TiAl(110). Therefore, the following orientation relationship results:

 $[001] Ti_3 AlC // [001] TiAl, (100) Ti_3 AlC // (100) TiAl, (020) Ti_3 AlC // (020) TiAl, (110) Ti_3 AlC // (110) TiAl.$

Figure 6(f) shows the IFFT image of the square area in Figure 6(c). As exhibited in Figure 6(f), the blue and red circles represent the TiAl and Ti₃AlC atoms, respectively. According to the atomic stacking sequence and the interface structure of Ti₃AlC and TiAl, it could be concluded that Ti₃AlC remains the coherent interface with TiAl during the precipitation.

Figure 7(a) shows the TEM image of the rod-like Ti_3AlC precipitate in TiAl alloys after growth. The selected area electron diffraction (SAED) pattern of the rod-like Ti_3AlC precipitate and TiAl is shown in Figure 7(b), and Figure 7(c) is the indexing of the FFT pattern in Figure 7(b). It could be observed that the large, bright spots represent the electron diffraction of TiAl and the small, dark spots represent the electron diffraction of Ti_3AlC .

The calibration result indicates that the Ti_3AlC is along the $[1\overline{1}0]$ zone axis, the TiAl is along the $[1\overline{1}0]$ zone axis, the $Ti_3AlC(001)$ is parallel to the TiAl(001), the $Ti_3AlC(111)$ is parallel to the TiAl(111). Thus, the orientation relationship is as follows:

 $[1\overline{1}0]Ti_3AlC//[1\overline{1}0]TiAl, \ (001)Ti_3AlC//(001)TiAl, \ (220) \\ Ti_3AlC//(220)TiAl, \ (111)Ti_3AlC//(111)TiAl.$

Figure 7(d) is the HRTEM image of the rod-like Ti₃AlC precipitate in Figure 7(a). Figure 7(e) and (f) shows the FFT pattern and IFFT image of the square area in Figure 7(d), respectively. It could be observed from Figure 7(e) that the interplanar spacing of Ti₃AlC(001) and Ti₃AlC (110) is 0.418 and 0.295 nm, respectively, which further proved that the rod-like precipitate is Ti₃AlC.

4 Discussion

In a nutshell, the C atoms solid-dissolved in the TiAl alloys will generate Ti₂AlC and Ti₂AlC nano-precipitates

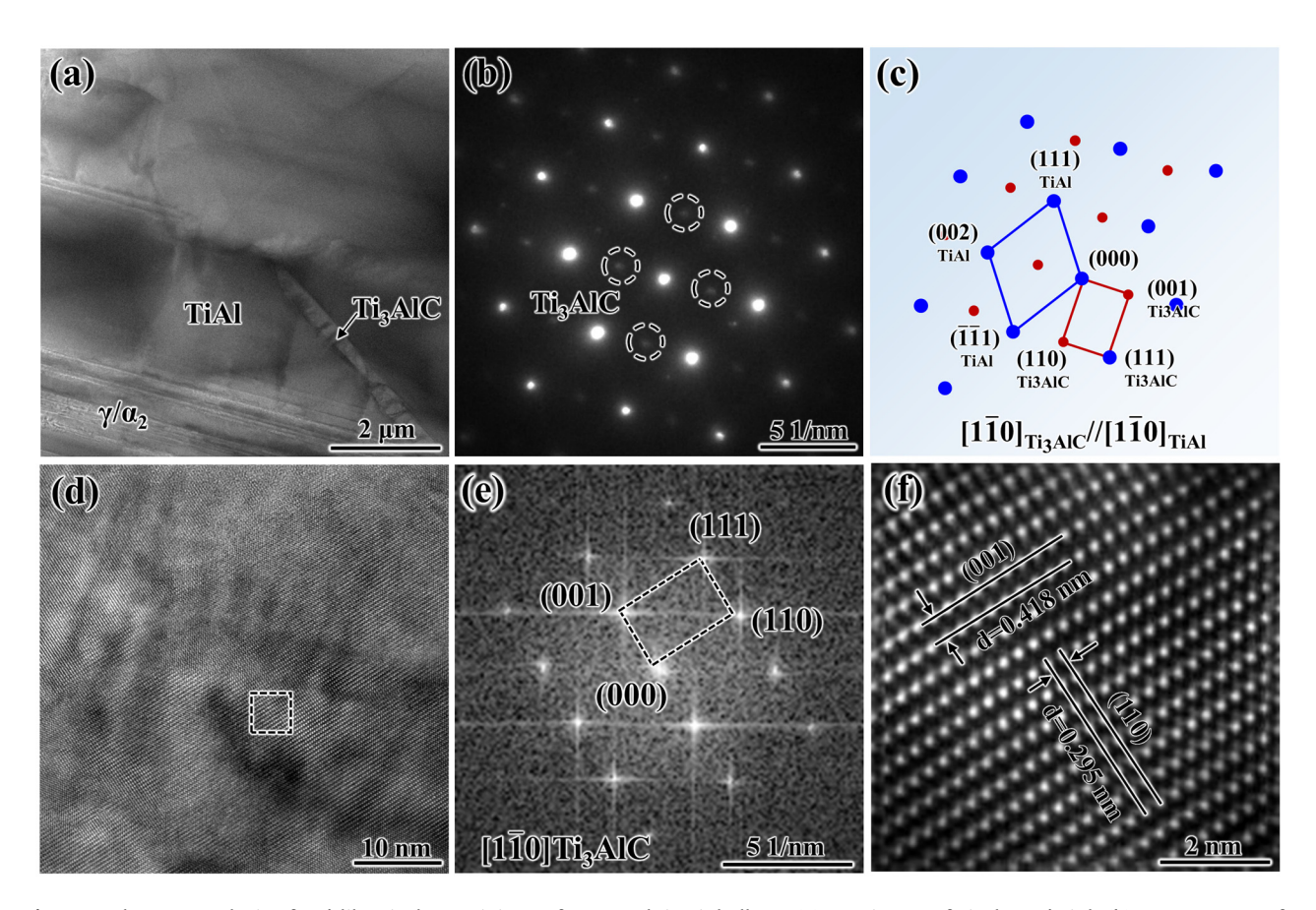


Figure 7: The TEM analysis of rod-like Ti₃AlC precipitate after growth in TiAl alloys: (a) TEM image of Ti₃AlC and TiAl; (b) SAED pattern of Ti₃AlC and TiAl; (c) indexing of the FFT pattern in (b); (d) TEM image of rod-like Ti₃AlC; (e) FFT pattern of Ti₃AlC; and (f) IFFT image of Ti₃AlC.

during the aging process, and their distribution, morphology, and orientation relationship with TiAl are quite different. Therefore, in the following sections 4.1 and 4.2, we attempt to explain the different morphology, distribution and orientation relationship between Ti₂AlC and Ti₃AlC nano-precipitates by investigating their crystal structures and lattice mismatch. The crystal structure and lattice parameters of TiAl, Ti₃Al, Ti₂AlC, and Ti₃AlC are demonstrated in Table 1.

4.1 Nucleation and growth mechanism of Ti₂AlC nano-precipitates

Previous research has shown that C atoms are inevitably solid-dissolved in the TiAl matrix during the aging process, and the concentration of C atoms in Ti₃Al is higher than that in TiAl. As reported by Menand et al. [25] using the advanced Atom Probe Technique (APT), the solid solution of C atom in Ti₃Al (0.15%, molar fraction) is 3–5 times higher than in TiAl. They tentatively concluded that the difference in solid solubility of C atom in Ti₃Al and TiAl is mainly due to the different interstitial vacancies occupied by C atom in the two-phase lattice. Scheu et al. [18] further investigated the interstitial vacancies of TiAl and Ti₃Al, and found that the C atom are mainly solidified in the octahedral interstitial of the TiAl and Ti₃Al, and the Ti₆-type is the best solid solution interstitial vacancy structure. Among them, Ti₃Al with DO₁₉ structure possesses this Ti₆-type octahedral interstitial, while the TiAl with L₁₀ structure contains Al₄Ti₂ and Al₂Ti₄-type octahedral interstitial, thus resulting in relatively higher solid solubility of C atoms in Ti₃Al. During the solid-phase transition stage, the lamellae of TiAl were first formed in Ti₃Al, and the TiAl/Ti₃Al lamellar colony was finally formed when the system reached the equilibrium state [26,27]. Because more defects distribute at the two-phase interface and the arrangement of atoms is loose, which is more beneficial to the enrichment of C atoms, the Ti₂AlC nano-precipitate tends to nucleate at the TiAl/Ti₃Al interface [28]. The formation process of the Ti₂AlC precipitate at the TiAl/Ti₃Al interface can be

described as follows: Ti₃Al → TiAl + Ti₃Al → TiAl + Ti₂AlC, and the process will be described in detail later through the schematic diagram of the atomic model. Furthermore, a small number of C atoms have segregated before diffusing to the grain boundary due to the effects of kinetics and thermodynamics, resulting in the precipitation of Ti₂AlC in TiAl and Ti₃Al. For the precipitation of Ti₂AlC in TiAl, the C atoms precipitate and form the segregation zone parallel to TiAl(111), which then promotes the nucleation of Ti₂AlC in this zone, as shown in Figure 2. The specific atomic planes of Ti₂AlC and TiAl(111) have a good match in the interface structure after nucleation. While for the precipitation in Ti₃Al, both the Ti₂AlC and Ti₃Al are hexagonal crystal structure and their chemical compositions have similar ratios of Ti and Al elements, thereby the Ti₂AlC with thermodynamically stable phase also tend to precipitate from Ti₃Al, as shown in Figure 4. It is worth noting that the precipitation of Ti₂AlC from Ti₃Al or TiAl is nucleated on the close-packed planes between them to minimize the interfacial energy.

Based on typical interface precipitation, Figure 8 shows the schematic diagram of the nucleation and growth behavior of Ti₂AlC nano-precipitates precipitated from the TiAl/Ti₃Al interface. Figure 8(a) is the atomic model of the TiAl/Ti₃Al interface, the red cube represents TiAl, the hexamorphic column represents Ti₃Al, and the blue cube represents the Ti₆-type octahedral interstice. First, the solid solubility of interstitial C atoms in Ti₃Al decreases with the decrease in temperature, thus making it easy to precipitate from the TiAl/Ti₃Al interface with more defects. Then, with the continuous precipitation of C atoms, under the influence of thermodynamics and kinetics, Ti₂AlC carbides are formed with the interface as the nucleation point, as shown in Figure 8(b). According to the crystal structure and the minimization of elastic strain energy, Ti₂AlC tend to form a good atomic matching with a coherent interface with the TiAl(111) and Ti₃Al(0001), *i.e.*, $TiAl(111)//Ti_2AlC(0001)//Ti_3Al(0001)$. Finally, the Ti_2AlC grow rod-like along the TiAl(111)/Ti₃Al(0001) interface, as shown in Figure 8(c). The formation reason for the rod-like morphology could be explained through the interface atomic model in Figure 8(d), the atomic models of closely packed TiAl(111) surface, Ti₂AlC(0001) surface, and Ti₃Al

Table 1: The crystal structure and lattice parameters of TiAl, Ti₂AlC, and Ti₃AlC

Phase	Crystal structure	Space group	<i>a</i> (nm)	b (nm)	<i>c</i> (nm)
TiAl	Tetragonal	P4/mmm (123)	0.4018	0.4018	0.4065
Ti₃Al	Hexagonal	P63/mmc (194)	0.5780	0.5780	0.4647
Ti ₂ AlC	Hexagonal	P63/mmc (194)	0.2968	0.2968	1.3223
Ti₃AlC	Cubic	Pm-3m (221)	0.4156	0.4156	0.4156

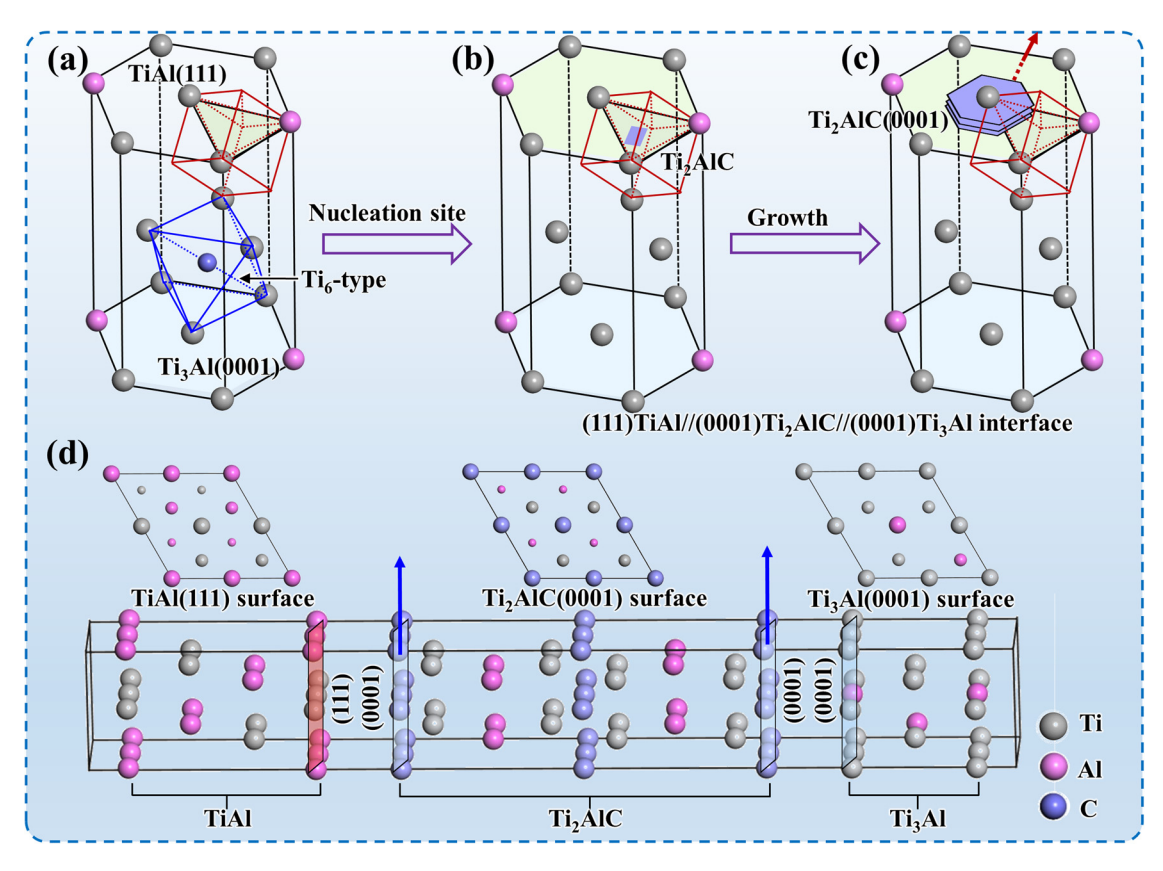


Figure 8: The schematic illustration for the nucleation and growth mechanism of Ti_2AlC nano-precipitates: (a) the $TiAl/Ti_3Al$ interface and Ti_3Al with Ti_6 -type octahedral interstice; (b) the nucleation of Ti_2AlC ; (c) the growth of Ti_2AlC ; and (d) the surface of TiAl(111), $Ti_2AlC(0001)$, and $Ti_3Al(0001)$ and the $Ti_3Al/Ti_3AlC/TiAl$ interface.

(0001) surface, and TiAl/Ti₂AlC/Ti₃Al interface. It could be seen that the Ti₂AlC(0001) is composed of the same kind of atoms, while along the [0001] direction it is composed of different kinds of atoms, and every two Ti₆C octahedra are separated by an Al layer along the [0001] direction. Due to the layered atomic arrangement, the growth rate of Ti₂AlC parallel to the (0001) plane is higher than that along the [0001] direction. In addition, it is worth mentioning that the Ti₂AlC precipitated at the TiAl/Ti₃Al interface can inhibit the further growth of the lamellae, thereby improving the stability of the structure, which is conducive to effectively improving the mechanical properties of the TiAl alloy [29,30].

4.2 Nucleation and growth mechanism of Ti₃AlC nano-precipitates

The Ti_3AlC nano-precipitates in this article preferentially grow into needle- and rod-like structures along the [001] TiAl during the nucleation and growth stage. Figure 9

shows the schematic diagram of the nucleation and growth of Ti₃AlC in TiAl. First, the dissolution of interstitial C atoms in the TiAl matrix tends to form the TiAl(C) solid solution with Al₂Ti₄-type octahedral interstices, as shown in Figure 9(a). Afterward, since the crystal structure and atomic arrangement of Ti₃AlC and TiAl(C) solid solution are quite close, as the thermodynamics gradually tends to the equilibrium state, the upper and lower Al atoms of the octahedral interstice are easily replaced by Ti atoms to form the initial Ti₃AlC with the TiAl(001) plane as the nucleation site. The Ti₃AlC precipitates maintain a coherent atomic correspondence with the interface between TiAl during the initial nucleation process, as shown in Figure 9(b). Figure 9(c) shows the growth model of Ti₃AlC and the needle-like direction corresponding to the TiAl[001]. The formation of needle-like morphology is mainly due to the fact that Ti₃AlC and TiAl have a lower lattice mismatch in the [001] direction than in the [100] and [010] directions. Li et al. [31] have calculated that the lattice mismatch between Ti₃AlC and TiAl is 3.13% along the [100] and [010] directions and 2.16% along the [001] direction. Therefore, it could be concluded

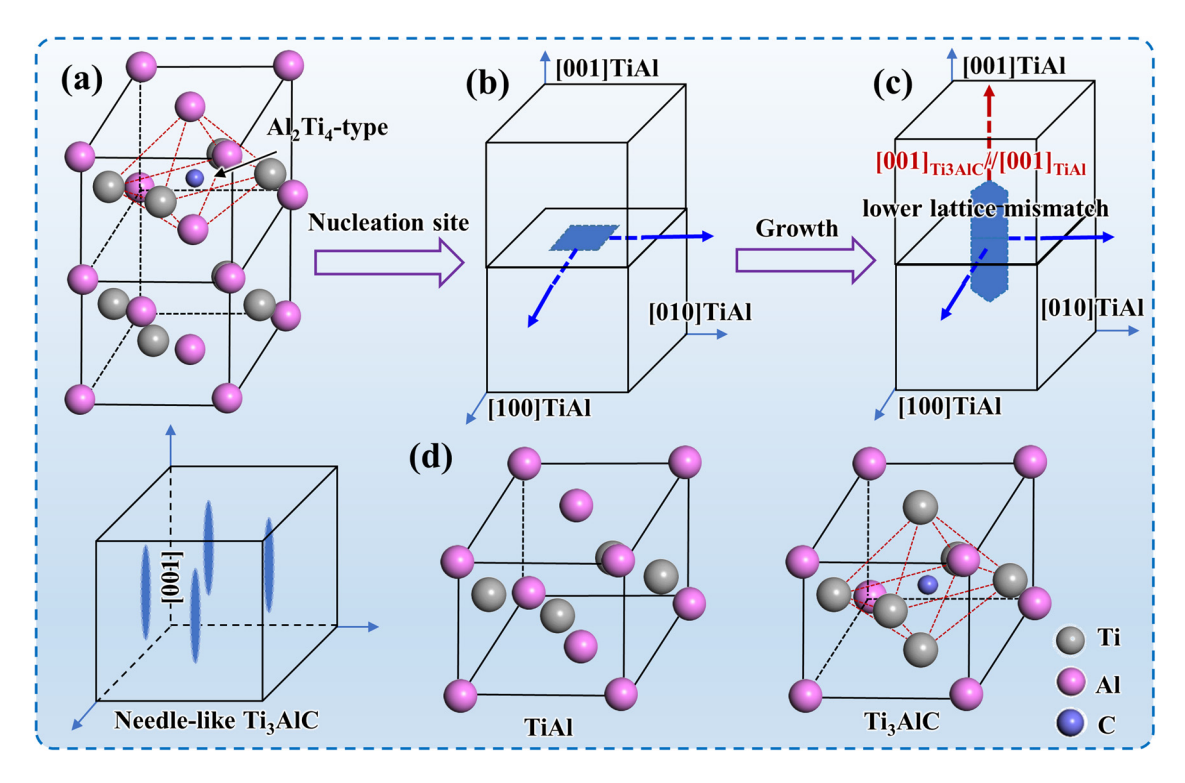


Figure 9: The schematic illustration for the nucleation and growth mechanism of Ti_3AlC nano-precipitates: (a) the atomic model of TiAl(C) solid solution with Al_2Ti_4 -type octahedral interstice; (b) the nucleation of Ti_3AlC ; (c) the growth of Ti_3AlC ; and (d) the atomic model of TiAl(C) and Ti_3AlC .

that the morphology of Ti₃AlC in TiAl is determined by the lattice mismatch between them. Furthermore, the lattice mismatch of the Ti₃AlC and TiAl is different at different precipitation stages. Considering the strain energy, the lattice mismatch between Ti₃AlC and TiAl is lower during the nucleation stage, and the elastic strain field between Ti₃AlC and TiAl is almost isotropic due to the small size of Ti₃AlC. The lattice mismatch further increases as the growth of the Ti₃AlC precipitates; thus, in order to decrease the strain energy at the interface, the Ti₃AlC needs to grow along the [001]TiAl direction, where the lattice mismatch is much lower. Figure 9(d) shows the atomic models of TiAl and Ti₃AlC, and it can be clearly seen that the atomic arrangements between them are quite similar, which further verifies the above phase transition process.

Based on the above analysis, the Ti_2AlC and Ti_3AlC nano-precipitates form the coherent interface (low-energy interface) with the TiAl matrix during precipitation, thereby reducing the overall free energy. It is worth mentioning that Ti_3AlC is a metastable phase, and the decomposition of Ti_3AlC at high temperatures will promote the nucleation and growth of Ti_2AlC with the increase in aging temperature and time. Therefore, it will be an interesting point to investigate the effect of carbide morphology evolution on the mechanical properties of TiAl alloys in the future.

5 Conclusions

In this article, the nucleation and growth behavior of Ti₂AlC and Ti₃AlC nano-precipitates were investigated by observing their distribution, morphology, and interface structure. The conclusions could be summarized as follows:

- 1) The needle-like C atom segregation zones in TiAl are the nucleation sites of Ti₂AlC precipitates, and the long axis direction of the segregation zones is parallel to the TiAl(111) plane.
- 2) The rod-like Ti_2AlC nano-precipitates mainly distribute at the $TiAl/Ti_3Al$ interface, and the orientation relationship between them is $[\bar{1}01]TiAl/[11\bar{2}0]Ti_2AlC/[11\bar{2}0]Ti_3Al$ and $(111)TiAl/(0001)Ti_2AlC/(0001)Ti_3Al$. Both the $Ti_2AlC/TiAl$ interface and the Ti_3Al/Ti_2AlC interface show good atomic matching, indicating that these interfaces are coherent.
- 3) The needle-like Ti₃AlC nano-precipitates distribute in TiAl with the orientation relationship of [001]Ti₃AlC//[001]TiAl, (100)Ti₃AlC//(100)TiAl, (020)Ti₃AlC//(020) TiAl, and (110)Ti₃AlC//(110)TiAl during the nucleation stage. While the orientation relationship between rod-like Ti₃AlC and TiAl is [110]Ti₃AlC//[110]TiAl, (001) Ti₃AlC//(001)TiAl, (220)Ti₃AlC//(220)TiAl, and (111) Ti₃AlC//(111)TiAl.

4) The lattice mismatch of Ti₃AlC and TiAl in the [001] direction is lower than in other directions during the nucleation and growth stages, thus both the needleand rod-like Ti₃AlC precipitates grow preferentially along the [001]TiAl direction.

Funding information: The authors acknowledge financial support from the National Natural Science Foundation of China (Grant No. 52101174).

Author contributions: All authors have accepted responsibility for the entire content of this manuscript and approved its submission.

Conflict of interest: The authors state no conflict of interest.

Data availability statement: All data generated or analyzed during this study are included in this published article.

References

- [1] Zheng G, Tang B, Zhao S, Wang WY, Chen X, Zhu L, et al. Evading the strength-ductility trade-off at room temperature and achieving ultrahigh plasticity at 800°C in a TiAl alloy. Acta Mater. 2022;225:117585.
- Naveed M, Renteria AF, Weiß S. Role of alloying elements during thermocyclic oxidation of β/y-TiAl alloys at high temperatures. J Alloys Compd. 2017;691:489-97.
- Tian S, He A, Liu J, Zhang Y, Zhang S, Zhang Y, et al. Investigation on the microstructure evolution and dynamic recrystallization mechanisms of TiAl alloy at elevated temperature. J Mater Res Technol. 2021;14:968-84.
- Perrut M, Caron P, Thomas M, Couret A. High temperature materials for aerospace applications: Ni-based superalloys and y-TiAl alloys. Comptes Rendus Phys. 2018;19:657-71.
- Kastenhuber M, Rashkova B, Clemens H, Mayer S. Effect of microstructural instability on the creep resistance of an advanced intermetallic γ -TiAl based alloy. Intermetallics. 2017;80:1-9.
- Zhang SZ, Zhao YB, Zhang CJ, Han JC, Sun MJ, Xu M. The microstructure, mechanical properties, and oxidation behavior of beta-gamma TiAl alloy with excellent hot workability. Mater Sci Eng A. 2017;700:366-73.
- Ma T, Li S, Wang Y, Wang X, Dong D, Zhu D. Phase transformation and dynamic recrystallization behavior of forged beta gamma TiAl alloy in variable thermomechanical conditions. J Mater Res Technol. 2022;18:4796-803.
- [8] Brotzu A, Felli F, Pilone D. Effect of alloying elements on the behaviour of TiAl based alloys. Intermetallics. 2014;54:176-80.

- Duan B, Yang Y, He S, Feng Q, Mao L, Zhang X, et al. History and development of y-TiAl alloys and the effect of alloying elements on their phase transformations. J Alloys Compd. 2022;909:164811.
- [10] Klein T, Schachermayer M, Mendez-Martin F, Schöberl T, Rashkova B, Clemens H, et al. Carbon distribution in multiphase y-TiAl based alloys and its influence on mechanical properties and phase formation. Acta Mater. 2015;94:205-13.
- Zhang T, Wu Z, Hu R, Zhang F, Kou H, Li J. Influence of nitrogen [11] on the microstructure and solidification behavior of high Nb containing TiAl alloys. Mater Des. 2016;103:100-5.
- Zollinger J, Lapin J, Daloz D, Combeau H. Influence of oxygen on solidification behaviour of cast TiAl based alloys. Intermetallics, 2007:15:1343-50.
- [13] Fang H, Chen R, Yang Y, Su Y, Ding H, Guo J, et al. Role of graphite on microstructural evolution and mechanical properties of ternary TiAl alloy prepared by arc melting method. Mater Des. 2018;156:300-10.
- [14] Song L, Hu X, Wang L, Stark A, Lazurenko D, Lorenz U, et al. Microstructure evolution and enhanced creep property of a high Nb containing TiAl alloy with carbon addition. J Alloys Compd. 2019;807:151649.
- Wang Q, Ding H, Zhang H, Chen R, Guo J, Fu H. Variations of microstructure and tensile property of γ -TiAl alloys with 0-0.5at% C additives. Mater Sci Eng A. 2017;700:198-208.
- [16] Li M, Xiao S, Chen Y, Xu L, Tian J. The effect of carbon addition on the high-temperature properties of β solidification TiAl alloys. J Alloys Compd. 2019;775:441-8.
- Menand A, Huguet A, Nérac-Partaix A. Interstitial solubility in γ and α_2 phases of TiAl-based alloys. Acta Mater. 1996;44:4729-37.
- [18] Scheu C, Stergar E, Schober M, Cha L, Clemens H, Bartels A, et al. High carbon solubility in a y-TiAl based Ti-45Al-5Nb-0.5C alloy and its effect on hardening. Acta Mater. 2009;57:1504-11.
- [19] Schwaighofer E, Rashkova B, Clemens H, Stark A, Mayer S. Effect of carbon addition on solidification behavior, phase evolution and creep properties of an intermetallic β-stabilized y-TiAl based alloy. Intermetallics. 2014;46:173-84.
- [20] Wu Z, Hu R, Zhang T, Zhang F, Kou H, Li J. Understanding the role of carbon atoms on microstructure and phase transformation of high Nb containing TiAl alloys. Mater Charact. 2017;124:1-7.
- [21] Lapin J, Pelachová T, Bajana O. High temperature deformation behaviour and microstructure of cast in-situ TiAl matrix composite reinforced with carbide particles. J Alloys Compd. 2019;797:754-65.
- [22] Benitez R, Kan WH, Gao HL, O'Neal M, Proust G, Srivastava A, et al. Mechanical properties and microstructure evolution of Ti₂AlC under compression in 25-1100°C temperature range. Acta Mater. 2020;189:154-65.
- [23] Liu P, Xie JP, Wang AQ, Ma DQ, Mao ZP. An interatomic potential for accurately describing the atomic-scale deformation behaviors of ${\rm Ti_2AlC}$ crystal. Comput Mater Sci. 2020;182:109757.
- [24] Zhan ZQ, Chen YX, Radovic M, Srivastava A. Non-classical crystallographic slip in a ternary carbide-Ti₂AlC. Mater Res Lett. 2020;8:275-81.

- [25] Menand A, Huguet A, Nérac-Partaix A. Interstitial solubility in γ and α_2 phases of TiAl-based alloys. Acta Mater. 1996;44:4729–37.
- [26] Chen YL, Yan M, Sun YM, Mei BC, Zhu JQ. The phase transformation and microstructure of TiAl/Ti2AlC composites caused by hot pressing. Ceram Int. 2009;35:1807–12.
- [27] Zghal S, Thomas M, Naka S, Finel A, Couret A. Phase transformations in TiAl based alloys. Acta Mater. 2005;53:2653-64.
- [28] Beyerlein IJ, Demkowicz MJ, Misra A, Uberuaga BP. Defectinterface interactions. Prog. 2015;74:125-210.
- [29] Lapin J, Kamyshnykova K, Pelachová T, Nagy Š. Effect of carbon addition and cooling rate on lamellar structure of peritectic TiAl based alloy. Intermetallics. 2021;128:107007.
- [30] Wang Q, Zeng L, Ding H, Chen R, Guo J, Fu H. Microstructures and mechanical properties of directionally solidified C-containing γ -TiAl alloys via electromagnetic cold crucible. Intermetallics. 2019;113:106587.
- [31] Li M, Xiao S, Xu L, Tian J, Chen Y. Microscale investigation of perovskite-Ti₃AlC strengthening and plastic deformation in high niobium containing TiAl alloys. J Alloys Compd. 2021;857:157563.